

“Step-up” versus “step-down” scattering asymmetry in the neutralization of H^- on free-electron vicinal metal surfaces

Boyan Obreshkov^{*}, Uwe Thumm

James R. Macdonald Laboratory, Department of Physics, Kansas State University, 116 Cardwell, Manhattan, KS 66506-2604, United States

Received 29 June 2006; accepted for publication 23 October 2006

Available online 13 November 2006

Abstract

The charge transfer between H^- and a free-electron vicinal metallic surface is studied using a wave-packet propagation method. We apply a statistical Thomas–Fermi–von Weizsäcker model with a local density approximation for the exchange–correlation energy to compute the ground-state electronic structure of the substrate. The long-range image charge effects in the electron transfer are included on a phenomenological level. We obtain the ion-survival probability from a rate equation for a set of realistic scattering trajectories of projectiles that are incident with a kinetic energy of 50 eV. Our calculations reveal a pronounced substrate orientation dependence of the charge transfer dynamics expressed in a “left–right” (or “step–up–step–down”) scattering asymmetry in the final ion-survival probability, which is caused by an enhancement of electron loss on the outgoing part of those ion trajectories which approach steps from below.

© 2006 Elsevier B.V. All rights reserved.

Keywords: Density functional theory; Charge transfer; Image potential; Vicinal surfaces

1. Introduction

When an ion or atom approaches a metallic surface, its electronic structure changes due to the perturbing fields of the substrate atoms. This results in the broadening and shift of the projectile energy levels [1]. The broadening is due to electron transfer between the projectile and the surface. The electron transfer process determines the final charge state of the projectile after reflection at the surface, while the direction of the transfer is given by the energies of the shifted projectile levels relative to the Fermi level of the substrate [2–4].

The formation and neutralization of ions in front of atomically flat surfaces has been studied in detail for more than a decade, and the main single-electron interaction mechanisms are fairly well understood [5–7]. The objective of this work is the calculation of the affinity level width and survival probability of H^- ions near a vicinal free-electron

surface. The detailed study of the effects related to the vicinal superstructure of the substrate is stimulated by recent experiments with stepped surfaces [8,9], where angle-resolved photoemission measurements revealed lateral electronic confinement in between surface steps. This confinement effect is attributed to both, the periodic step structure, which builds up an effective confining lateral potential, and the surface projected bulk band gap, which prevents fast tunnelling decay of the confined electrons into the bulk of the substrate. More recently, scanning tunnelling microscopy (STM) measurements [10] have clearly revealed the presence of localized dipole moments near the step edges of vicinal surfaces. These dipoles are due to the Smoluchowski effect, i.e., the redistribution of electronic density near steps in response to the incomplete screening of positive ion cores by conduction electrons. These measurements provide independent information about the formation of confining electronic potentials at the steps.

In the present paper, we describe the electron transfer process in terms of the tunnelling of a single active electron

^{*} Corresponding author. Tel.: +1 785 532 1642.

E-mail address: obreshko@phys.ksu.edu (B. Obreshkov).

through the potential barrier separating the projectile from the substrate. The electronic motion is modelled quantum mechanically, and the projectile center-of-mass is assumed to move classically. To evaluate the surface potential felt by the active electron, we adopt the jellium approximation, in which the charge distribution of the ionic cores is replaced by a positive uniform background charge. The screening density of the substrate valence electrons is calculated self-consistently within the Thomas–Fermi–von Weizsäcker (TFvW) model in local density approximation (LDA) for the exchange–correlation energy. Since the LDA approximation does not exhibit the correct asymptotic image attraction at large distances from the surface, we correct and extend our model by including the image charge effects phenomenologically.

The projected density of states (PDOS) of the ion–surface system is evaluated by numerical propagation of the time-dependent two-dimensional Schrödinger equation for the motion of the electronic wave packet in the collision plane of the projectile, assuming adiabatic (quasistatic) conditions for the projectile’s motion hold. We evaluate the static shift and width of the ion–affinity level by fitting the Breit–Wigner resonance profile to the PDOS. The H^- survival probability after reflection from the surface is calculated from the static resonance width within a rate-equation approach for a set of realistic trajectories of the projectile, including both electron capture from and electron loss to the substrate. Although the constrained dimensionality of our model (2D) does not directly correspond to an experimental situation, it allows us to study some important aspects of the resonant charge transfer dynamics at vicinal metallic surfaces. The various approximations employed in our model are discussed.

The plan of this paper is as follows. In Section 2 we describe the theoretical formalism. In Section 3 we discuss our numerical results for the electronic structure of the surface and its consequences for the charge exchange dynamics between slow H^- ions and a double-stepped free-electron vicinal surface. Section 4 contains our main conclusions. Unless otherwise stated, we use atomic units ($e = \hbar = m_e = 1$).

2. Theoretical model

Fig. 1 illustrates the geometry of the vicinal surfaces used in our calculations within the jellium model. The positive background charge density has a lateral periodic modulation in the optical plane defined by the terrace length $L = ma_0$ and the step height $H = na_0$, where $a_0 = 3.41$ is the lattice spacing between the atomic planes with (001) orientation and (m, n) is a pair of integer numbers. The face of a ledge is orthogonal to the faces of the two adjacent terraces and the surface has translational invariance in the step-edge direction. This configuration corresponds to a face-centered cubic $m(001) \times n(100)$ vicinal crystal, according to [11]. In our numerical applications the surface geometry is specified by a corrugation function

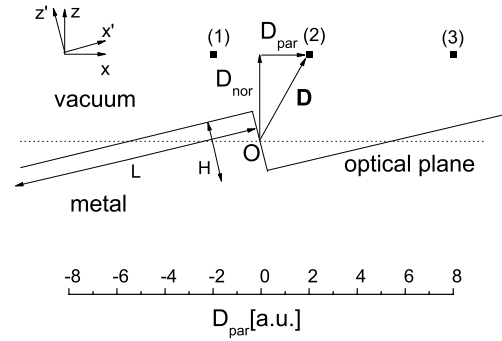


Fig. 1. Geometry of a free-electron vicinal surfaces with step length L and step height H . The optical surface plane is indicated by a dotted line. The ion position vector in front of the surface is $\mathbf{D} = (D_{\text{nor}}, D_{\text{par}})$. The points 1–3 are situated on a plane parallel to the optical surface. Positions 1 and 2 of the ion are near the upper corner of the step, position 3 is in the valley between the steps (see text).

$\zeta(x)$. The jellium background charge density of the nuclei is assumed to follow the surface corrugation by occupying the space $z < \zeta(x)$, where (x, z) are Cartesian coordinates parallel and perpendicular to the optical surface plane. The projected density of states of the H^- –surface system is calculated for a sequence of fixed parallel positions D_{par} of the ion at a fixed distance D_{nor} in front of the optical surface as shown in Fig. 1. The points (1) and (2) correspond to parallel positions near the top step edge, and position (3) is between the steps. In our calculations we also employ a second reference frame denoted with primed coordinates (x', z') , which is obtained after rotation in the (x, z) –plane by the miscut angle $\alpha = \arctan(n/m)$.

We describe the charge-transfer process by solving the two-dimensional time-dependent Schrödinger equation for the motion of the active electron in the collision plane of the projectile,

$$i\partial_t \Psi(t) = H\Psi(t), \quad H = T + V(x, z), \quad (1)$$

where T is the two-dimensional kinetic energy operator for the electron. The potential energy of the electron is expressed as

$$V = V_{e-H} + V_{e-surf}, \quad (2)$$

and contains the electron–hydrogen interaction potential, V_{e-H} , and the electron–surface interaction potential in the absence of the hydrogen core, V_{e-surf} . The transition amplitude for charge transfer is calculated in adiabatic approximation for the motion of the ion, i.e., for an arbitrary but fixed ion position,

$$A(t; \mathbf{D}) = \langle \Psi(0) | \Psi(t; \mathbf{D}) \rangle, \quad (3)$$

where $|\Psi(0)\rangle$ represents the initial unperturbed state of H^- , and \mathbf{D} is the position vector of the center-of-mass of the projectile in the collision plane. The position E_r , width Γ , and amplitude a of an isolated adsorbate-induced resonance in the ion–surface system are obtained by fitting the PDOS

$$\rho(E; \mathbf{D}) = \frac{1}{\pi} \text{Re} \int_0^{\infty} dt e^{iEt} A(t; \mathbf{D}), \quad (4)$$

to a Lorentzian curve and a constant non-resonant background contribution ρ_0

$$\rho = \rho_0 + a \frac{\Gamma/2}{(E - E_r)^2 + \Gamma^2/4}. \quad (5)$$

The PDOS is calculated by numerical integration of the Schrödinger equation (1) using the Crank–Nicholson propagation method [7,12].

Negative-ion-survival probabilities P are calculated from a rate-equation for a set of trajectories for incident projectiles with a kinetic energy of 50 eV,

$$\frac{dP}{dt} = -g_{\text{loss}} \Gamma_{\text{loss}}[\mathbf{D}(t)]P + g_{\text{cap}} \Gamma_{\text{cap}}[\mathbf{D}(t)](1 - P). \quad (6)$$

The electron loss and capture rates Γ_{loss} and Γ_{cap} are determined in compliance with the Pauli-exclusion principle, and the spin-statistical factors for loss and capture are $g_{\text{loss}} = 2$ and $g_{\text{cap}} = 1$ (capture can occur only into the ground state of H^- , which is a spin singlet). Γ_{loss} and Γ_{cap} are set equal to either the static width Γ or zero, depending on the relative energetic position of the shifted affinity level and the Fermi level and are evaluated along the classical trajectory of the incident ion $\mathbf{D}(t)$. For a given angle of incidence Θ_{inc} of the H^- ion with respect to the optical plane, we evaluate the classical trajectory based on a Thomas–Fermi–Moliere interatomic potential [13], including the effects of the surface corrugation.

The effective potential of the hydrogen core in (2) is represented by an effective central potential [14], including a screened short-range Coulomb part and a long-range polarization part,

$$U(r) = -(1/r) \exp(-2r) - (\alpha/2r^4) \exp(-\beta/r^2). \quad (7)$$

In this equation, r is the radial distance from the nucleus, and $\alpha = 9/2$ is the ground-state polarizability of hydrogen. This potential is regularized and the parameter β is adjusted numerically such that the diagonalization of $V_{\text{e-H}}$ on a two-dimensional numerical grid holds a single weakly bound state with an electron affinity of 0.76 eV [7].

We model the electron–surface interaction potential $V_{\text{e-surf}}$ within the TFvW approach [15–17] as in our earlier study [12], i.e. as a sum of the electrostatic Hartree potential of the electronic and nuclear charges and the effective local exchange-correlation potential

$$V_{\text{e-surf}}(\mathbf{r}) = \int d^3 \mathbf{r}' \frac{n_0(\mathbf{r}') - n_{\text{J}}(\mathbf{r}')}{|\mathbf{r} - \mathbf{r}'|} + \left. \frac{\delta E_{\text{xc}}^{\text{LDA}}[n]}{\delta n(\mathbf{r})} \right|_{n=n_0}. \quad (8)$$

n_0 is the density of the valence electrons that minimizes the total ground-state TFvW energy density functional, n_{J} is the jellium background charge density, and $E_{\text{xc}}^{\text{LDA}}$ is the local density approximation for the exchange-correlation energy of the electronic system.

The (polarization) image charge effects are introduced in our model by χ^2 -fitting the analytical long-range model

potential $V_{\text{l.r.}}$ proposed by Jennings–Jones [18] to the planar averaged self-consistent von-Weizsäcker (short-range) potential $V_{\text{s.r.}} = \int_{-L/2}^{L/2} dx V_{\text{e-surf}}(x, z)/L$. The potential $V_{\text{l.r.}}$ merges into the classical electrostatic image potential $-1/4z$ as $z \rightarrow \infty$ and is characterized by the three parameters U_0 , λ , and z_0 : z_0 specifies the effective image-charge plane location [19] with respect to the optical plane, λ determines the range over which the surface barrier saturates in vacuum, and U_0 is the constant bulk potential in the metal interior. Including the image charge effects, the effective electron–vicinal surface interaction potential is then redefined according to

$$V_{\text{e-surf}}^{\text{new}}(x, z) = V_{\text{e-surf}}^{\text{old}}(x, z) + V_{\text{l.r.}}(z) - V_{\text{s.r.}}(z), \quad (9)$$

where $V_{\text{e-surf}}^{\text{old}}$ is the numerical LDA potential from Eq. (8).

3. Results and discussion

In this section, we present our numerical results for the affinity level shift and width and survival probability for H^- ions in front of free-electron vicinal surfaces, corresponding to a bulk Wigner–Seitz radius $r_s = 2.7$, which approximately represents a Cu crystal. This particular choice is dictated by the availability of experimental data on vicinal Cu surfaces [8,9]. Although Cu is a transition metal known to exhibit non-free electron properties, the present study will not take into account more detailed characteristics of the Cu-electronic structure. Instead, we will focus on the effects on the electron transfer dynamics that are due to the surface superstructure (here: steps). This will help us, in a future investigation, to quantify the importance of the (both separate and combined) effects of surface superstructure and the electron reflectivity that is imposed by the (L - or X -) band gap of a real Cu surface.

3.1. Electronic structure calculation

Fig. 2(a) shows a contour map of the electron density n/n_{b} normalized to the bulk density $n_{\text{b}} = 3/4\pi r_s^3$ for a double stepped jellium surfaces with $(m, n) = (8, 2)$. Due to the Smoluchowski effect [20], the electronic density spills out from the top of the step into the valley between the upper and lower terrace, forming a permanent electric dipole that is localized near the edge. The non-uniformity of the electronic density in vicinity of the step varies laterally over a distance approximately given by the Thomas–Fermi screening length $l_{\text{TF}} = k_{\text{F}}/(12\pi n_{\text{b}})^{1/2} = 1.05$ where the momentum on the top of the Fermi distribution is $k_{\text{F}} = (3\pi^2 n_{\text{b}})^{1/3} = 0.71$. The electrostatic Hartree potential derived from this density distribution is shown in Fig. 2(b). Due to the electron depletion from the step edges, the electrostatic field of the top edge ionic cores is incompletely screened and penetrates into the vacuum side of the interface. Similarly, the bending of the equipotential lines towards the lower corner of the step is due to the electron density increase in this domain.

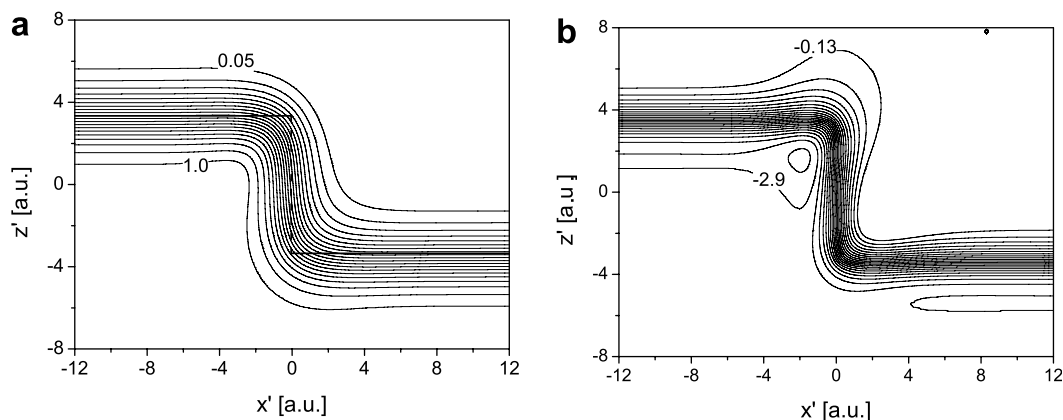


Fig. 2. Contour maps of the normalized electron charge density $n(x', z')/n_b$ for a free-electron vicinal Cu surface with $(m = 8, n = 2)$ (a) and the electrostatic Hartree potential $\phi(x', z')$ (b). The coordinates x' and z' are oriented parallel and perpendicular to the terrace. The contour-line spacing is 0.05 (a) and 0.095 eV (b). The dashed-line indicates the jellium edge.

The localized step dipole moment has a dominant component perpendicular to the terrace and is oriented towards the vacuum (Fig. 2(a)), i.e., opposite to the direction of the dipole moment distributed over the terraces. This step dipole slightly reduces the dipole moment on the flat terrace and thus leads to a decrease of the metallic work-function W relative to the work function of a flat surface W_{flat} . Our numerical results for the work function change $\Delta W = W_{\text{flat}} - W$ for several Cu surface morphologies are shown in Table 1. Our independent calculation [12] of the work function within the TFvW model for atomically flat Cu surface yields $W_{\text{flat}} = 3.35$ eV.

The work function change is small and decreases linearly with the increase of the step density, in agreement with the measured linear decrease of the work function [24]. This effect is also apparent in Fig. 3 where the electrostatic Hartree potentials for a flat surface and the averaged over the volume of an unit-cell potential $\bar{V}_H(z) = \int_{-L/2}^{L/2} dx V_H(x, z)/L$ for a vicinal Cu surface with $(m = 8, n = 2)$ are shown. The small, but systematic shift of the bulk level of the vicinal potential relative to the electrostatic potential of the atomically flat Cu surface determines the overall decrease of the work function due to the step-induced dipole (Table 1). Our numerical results for the work function change are

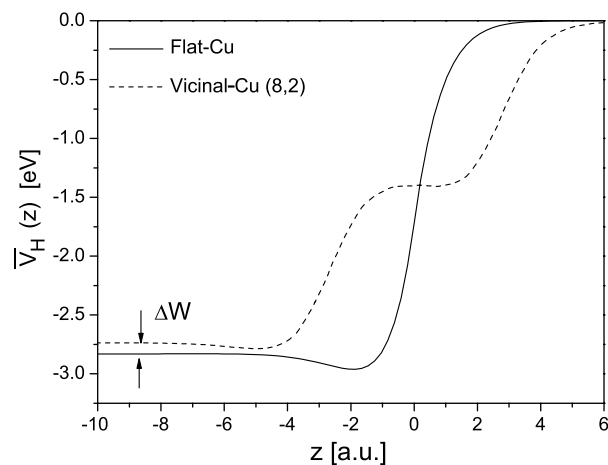


Fig. 3. The electrostatic Hartree potential in eV for a flat Cu surface (solid line) and the unit-cell averaged Hartree potential for the $(m = 8, n = 2)$ Cu vicinal surface (dashed line).

in a very good quantitative agreement with the *measured* values for the work function decrease at vicinal Cu surfaces. In Refs. [21,25] the measurements for the work-function of the Cu(117) (with $L = 17.2$) and Cu(119) ($L = 21.9$) vicinal surfaces relative to the atomically flat

Table 1

Our calculated work function W and work function change ΔW in eV for a single-stepped and double-stepped free-electron vicinal Cu surfaces in comparison with theoretical data of Ref. [23] and experimental results of Refs. [21,22]

L	W	ΔW	Reference	Morphology
20.5	3.28 (3.24)	0.07 (0.11)	This work	Stepped jellium
27.3	3.30 (3.27)	0.05 (0.08)	This work	Stepped jellium
34.1	3.32 (3.28)	0.03 (0.07)	This work	Stepped jellium
40.9	3.35 (3.30)	0.00 (0.05)	This work	Stepped jellium
17.2	4.60	0.04	[21]	Cu(117)/Cu(001)
21.9	4.59	0.03	[21]	Cu(119)/Cu(001)
26.5		0.04	[22]	Cu(775)/Cu(111)
24.4	4.48	0.41	[23]	Cu(532)/Cu(111)

The first column specifies the terrace period L in a.u. The second column specifies the work function for a single (double) step, and the third column the work function change for a single (double) step. The numbers in the brackets refer to the double-stepped vicinal surfaces. The density parameter is $r_s = 2.7$.

Cu(001) surface reveal a decrease by $\Delta W = 0.04$ and 0.03 eV, respectively. The measured small decrease of the work-function is also evident from Ref. [22], where the authors report $\Delta W = 0.04$ eV for the Cu(775) (with $L = 26.5$) vicinal relative to the flat Cu(111) surface.

Our results for the work-function change disagree with more detailed DFT calculations that are based on a generalized-gradient approximation for the exchange-correlation energy and use an ultrasoft Vanderbilt pseudopotential for the description of the localized ionic cores [23]. In Ref. [23], the calculated work function decrease for the Cu(532) vicinal surface (with $L = 24.4$) relative to the flat Cu(111) surface is $\Delta W = 0.41$ eV. From the work function change we estimate the magnitude of the component of the step dipole perpendicular to the terrace d_{\perp} by using the Helmholtz formula [24] $\Delta W = 4\pi N_s d_{\perp}$ where $N_s = \tan\alpha/a_0$ is the number density of surface steps. This formula is approximately valid for low densities of the steps. For $(m, n) = (8, 2)$ we obtain $d_{\perp} = 0.02D$ ($1D = 3.3 \times 10^{-30}$ C m). This indicates that the charge density redistribution at the steps is a microscopic effect. We therefore do not expect the overall work-function change to have a significant influence on the electron charge transfer dynamics.

The self-consistent electron–surface interaction potential $V_{e\text{-surf}}$ is shown in Fig. 4(a). The potential has a steep gradient near the top edge and varies more slowly near the lower corner of the step, due to the above-mentioned Smoluchowski redistribution. The image charge corrected potential is shown in Fig. 4(b). This long-range potential is determined from the one-dimensional fit of the Jennings–Jones model to our numerical planar averaged LDA potential, as described in Section 2. In our fit $U_0 = 0.37$ is held fixed and for the optimized values of the remaining two parameters we have $\lambda = 0.66$ and $z_0 = 2.01$. The difference potential $V_{\text{diff}} = V_{\text{l.r.}} - V_{\text{s.r.}}$ shown in Fig. 5 is then used to redefine the two-dimensional surface potential, according to Eq. (9). All subsequent results are obtained from the image charge corrected electron–surface interaction potential (Fig. 4(b)).

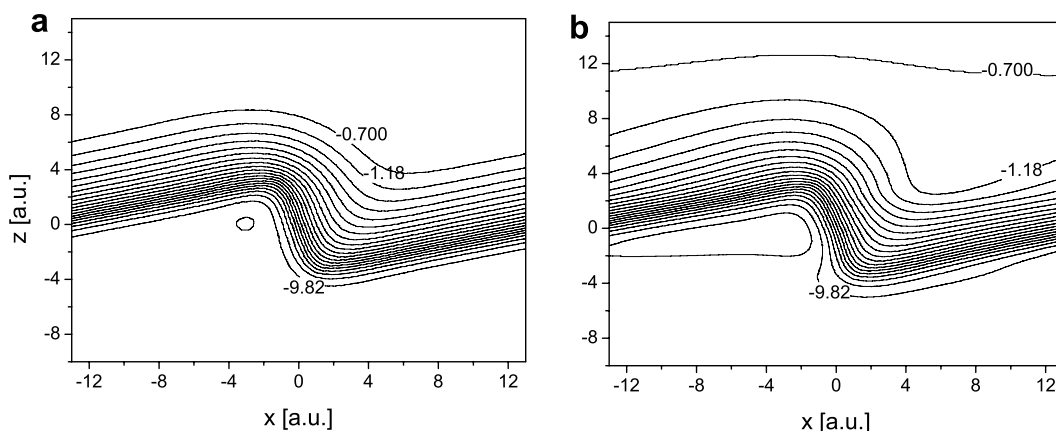


Fig. 4. Contour map of the self-consistent field $V_{e\text{-surf}}$ for a free-electron Cu vicinal surface with $(m = 8, n = 2)$ without (a) and with (b) the inclusion of the image-charge effects. The contour-line spacing is 0.48 eV. The labels give potential energies relative to the vacuum level.

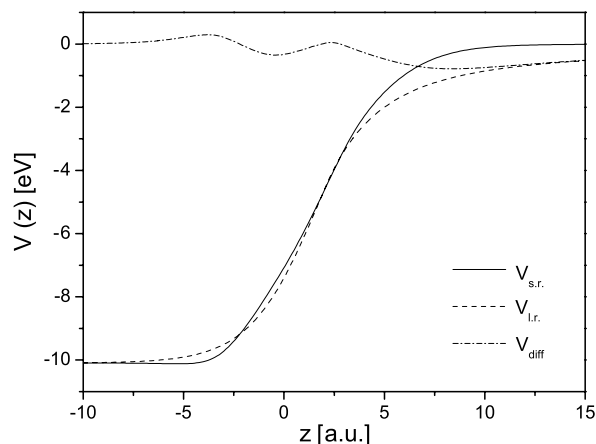


Fig. 5. Comparison of the average effective potential energy for an electron near a double stepped vicinal jellium surface $V_{s,r}$, obtained within the Thomas–Fermi–von Weizsäcker model (dotted line) and the model Jennings–Jones potential $V_{l,r}$ (solid line). The dashed-dotted line corresponds to the difference potential $V_{\text{diff}} = V_{l,r} - V_{s,r}$. The Wigner-Seitz radius is $r_s = 2.7$.

3.2. Projected density of states, shift and width of the ion level

The shift and width of the affinity level are obtained after calculating the PDOS from (4). The PDOS for a vicinal Cu surface with a morphology specified by $(m, n) = (8, 2)$ is shown in Fig. 6(a) for an H^- ion positioned at $D_{\text{nor}} = 10$. At such large distances the affinity level resonance appears as a Lorentzian peak in the PDOS far above the Fermi energy level $E_F = -3.27$ eV with a width due to electron loss into the unoccupied bulk metallic states. The resonance level width and shift depend sensitively to the lateral variation of the surface potential. Near position (3) ($D_{\text{par}} = 8$), the width due to resonant charge transfer is $\Gamma = 0.08$ eV. Approaching a step edge (position (2), $D_{\text{par}} = 2$) the width gradually changes to 0.24 eV, and above a step edge (position (1), $D_{\text{par}} = -2$), the width acquires a local maximum of 0.39 eV. The shift of the ion level follows only on average

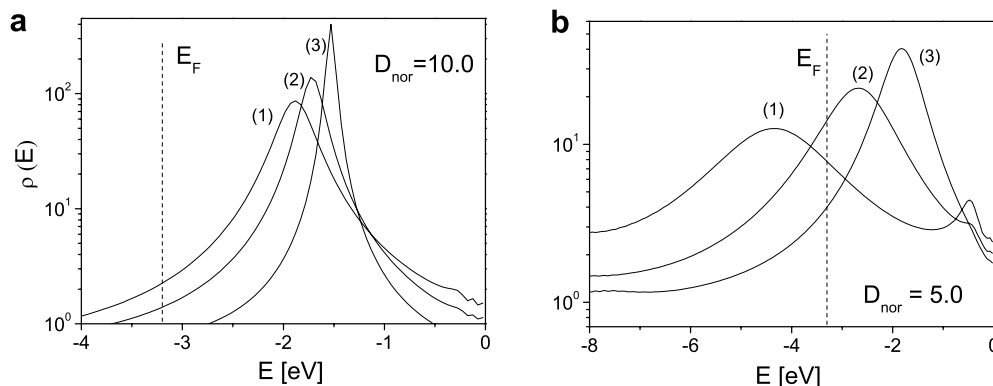


Fig. 6. Projected density of states for H^- in front of a free-electron vicinal Cu surface with $(m, n) = (8, 2)$. The normal coordinate of the ion is $D_{\text{nor}} = 10$ a.u. (a) and $D_{\text{nor}} = 5$ a.u. (b). The lateral positions of the ion (1)–(3) are indicated in Fig. 1.

the image potential shift $-1/4(D_{\text{nor}} - z_0)$. When the projectile moves closer to the surface, at $D_{\text{nor}} = 5$ (Fig. 6(b)), the ion level appears largely broadened with small amplitude. The width Γ of the affinity level is 0.78 eV in the valley between the terraces at position (3), where the charge exchange is due to electron loss from the ion to the surface. The transfer rate increases to $\Gamma = 1.44$ eV approaching the upper corner of the step (position (2)), where the affinity level is nearly degenerate with the Fermi level of the substrate. Above the step edge (position (1), the charge transfer reverses its direction to electron capture into to the H^- affinity level from the delocalized bulk states of

the substrate, since the ion level is shifted across and below E_F . The width (or the capture rate) at this distance near the edge is quite large, $\Gamma = 2.21$ eV. At the same distance ($D_{\text{nor}} = 5.0$, position (1)) a new resonance state appears in the high-energy part of the spectrum at $E = -0.41$ eV. It has a small amplitude of presence near the projectile and is relatively short-lived, with a width $\Gamma \approx 0.7$ eV. We attribute this feature in the PDOS to the population of the lowest image state of the substrate. Due to the absence of a band gap in our model, this state is degenerate with the unoccupied conduction band states and decays into the bulk via resonant charge transfer.

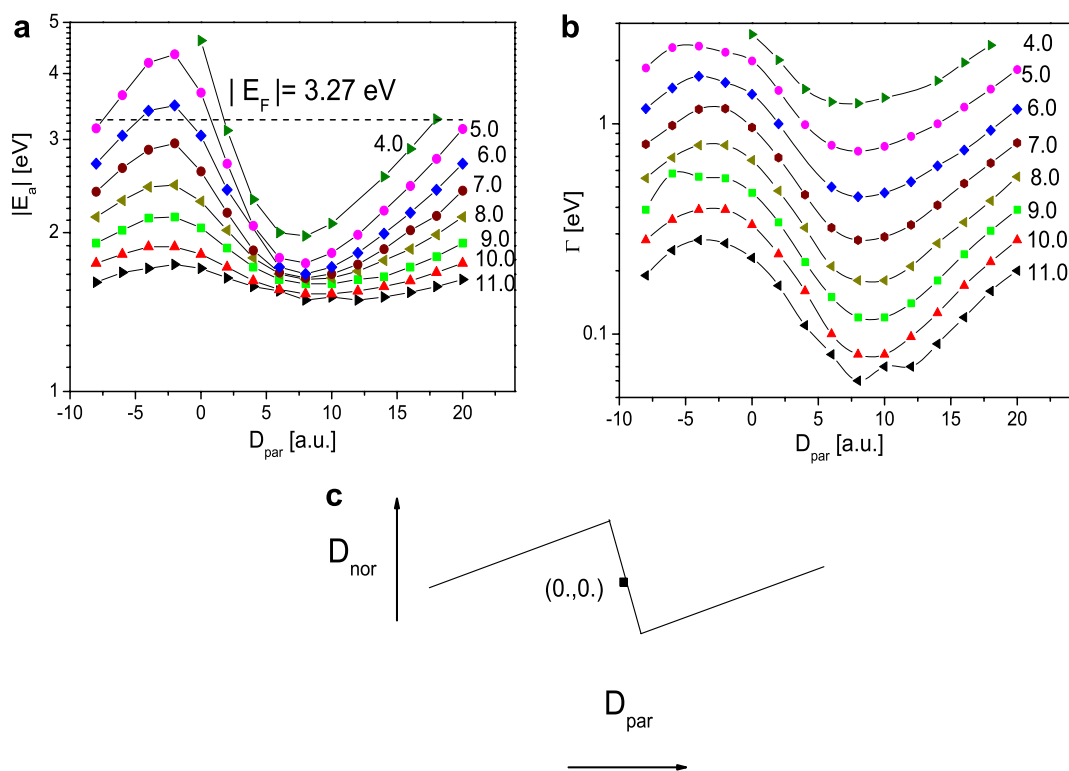


Fig. 7. Absolute value of the energy (a) and the width (b) of the H^- affinity level as a function of the ion position ($D_{\text{nor}}, D_{\text{par}}$) in front of a free-electron vicinal Cu surface with $(m, n) = (8, 2)$. The numbers attached to each curve indicate the distance D_{nor} (in a.u.) of the ion in front of the optical surface plane. The dashed line in (a) denotes the position of the Fermi energy level of the substrate. The vicinal surface geometry near the step is schematically shown in (c).

The energy and width of the affinity level resonance obtained from the PDOS for H^- in front of a Cu vicinal surface with $(m, n) = (8, 2)$ are shown in Fig. 7(a). The width clearly exhibits the vicinal structure of the surface, oscillating laterally and decaying exponentially towards the vacuum side of the interface. For $D_{\text{nor}} > 2$ and in the valley between the terraces, the transfer between the ion and the surface is blocked, Γ acquires a local minimum. Thus charge exchange always corresponds to “slow” electron loss from the ion to the surface. And the affinity level is repelled from and cannot cross the Fermi energy level of the substrate (Fig. 7(b)). Near the step edges and at distances below $D_{\text{nor}} \approx 5$, the charge exchange rate is significantly enhanced. When the energy of the resonance state shifts across and below the Fermi level, charge transfer corresponds to fast capture of an electron into the ion level from the conduction band of the metal. These gross features of the electron transfer at vicinal free-electron surfaces are further analyzed in the following subsection within the wave packet propagation method.

3.3. Wave packet propagation for fixed ion position

Fig. 8(a)–(d) present the electronic wave packet at four different instants of time 0, 50, 150, and 600 for the jellium vicinal Cu surface with $(m, n) = (8, 2)$. The ion is situated between the terraces near the lower corner of the step corresponding to $D_{\text{par}} = 8.0$ at $D_{\text{nor}} = 8.0$ (see also Fig. 1). The logarithm of the probability density $|\Psi|^2$ is plotted as a function of the lateral and parallel electronic coordinates. Fig. 8(a) shows the initial unperturbed bound state of the H^- ion at time $t = 0$. At $t = 50$ (Fig. 8(b)), the electronic wave packet tunnels into the metal in the two directions, where the surface barrier is most transparent. This is a direct consequence of the Smoluchowski smoothing of the unperturbed electron density of the substrate near the edges. The charge transfer towards to lower corner of the step is blocked due the larger barrier width seen by the electron. Consequently the decay of the wave packet occurs through the terrace and the upper corner of the nearest step, where the surface barrier for tunnelling is reduced. At larger times, $t = 150$ (Fig. 8(c)), the electron has already built up the wave function of the quasistationary state and its density decays in two well separated jets. A major part of the wave function remains localized near the core of H^- due to the above mentioned blocking of the transfer towards the lower corner of the step. At very large times, $t = 600$ (Fig. 8(d)), an essential part of the packet has tunneled into the bulk and the electronic flux of outgoing probability remains distributed in the two jets, the flux being more intensive in direction perpendicular to the terrace. The oscillations with a large period of 9–10 a.u. seen in Fig. 8(c) are attributed to the interference of the outgoing waves leaving the quasistationary state and the non-resonant background contribution, generated due to the projection of the initial wave-packet on the eigenfunctions of the ion-surface Hamiltonian.

Fig. 8(e)–(g) show the electronic wave packet at three different times 0, 50, and 150, corresponding to a negative ion situated near a step edge with coordinates $D_{\text{par}} = 2.0$ and $D_{\text{nor}} = 8.0$. Fig. 8(e) shows again the initial bound state of the H^- ion. At small times, $t = 50$, the electron is seen to tunnel and delocalize through the upper corner of the step, where the surface barrier is most transparent. At larger times, $t = 150$, the H^- decays according to its static width, corresponding to an outgoing flux into the metal in the direction determined by the line connecting the position of the negative ion with the nearest top step edge on the surface. Noticeably, the atomic and bulk parts of the wave-function have an equal amplitude as a consequence of the large transparency of the surface barrier in this direction. At much larger times, $t = 600$ (not shown), the wave packet has entirely left the hydrogenic core. It is now completely absorbed at the numerical grid boundaries.

From Fig. 8(c), (d) and (g), we can see that the negative ion decay is different near the top edge of a step and in between two adjacent terraces: the quasistationary state is long-lived when the ion is in the valley between the terraces due to the Smoluchowski modulation of the transparency of the surface barrier, suppressing the charge transfer towards the lower corner of the step. In contrast, the affinity resonance becomes short-lived in the vicinity of a top edge of the step, where the electron makes a direct transition into the bulk through the reduced barrier seen at this position of the ion (see also Fig. 4(a) and (b)).

The above description of the electron dynamics is approximate and corresponds to the decay of the negative ion into a two-dimensional continuum of jellium metallic states. A quantitative estimate of the effects related to the step edge degree of freedom (the motion along the y -axis) of the electron is not given at this stage, since 3D calculations would involve a large computational effort. However, we note that due to the blocking of the electron motion towards the lower corner of the step, the decay into the top step edge electronic continuum may become important. The coupling to this one-dimensional continuum will be even more emphasized in the presence of a band gap, which will prevent fast propagation of the electron through the lower terrace, such that the step will guide the electronic motion in between the terraces and along the edge of the surface.

3.4. Neutralization of moving ions

The dynamic study of the charge transfer in our approach is based on the rate Eq. (6). In this approximation it is assumed that on the characteristic time scale over which the projectile’s motion changes, the electron has always enough time to tunnel through the barrier, explore the potential, and built up the wave function of the quasistationary state. The applicability of this adiabatic approximation is discussed elsewhere [26,27].

The survival probability of H^- in collision with a stepped Cu surface with $(m, n) = (8, 2)$ is calculated along

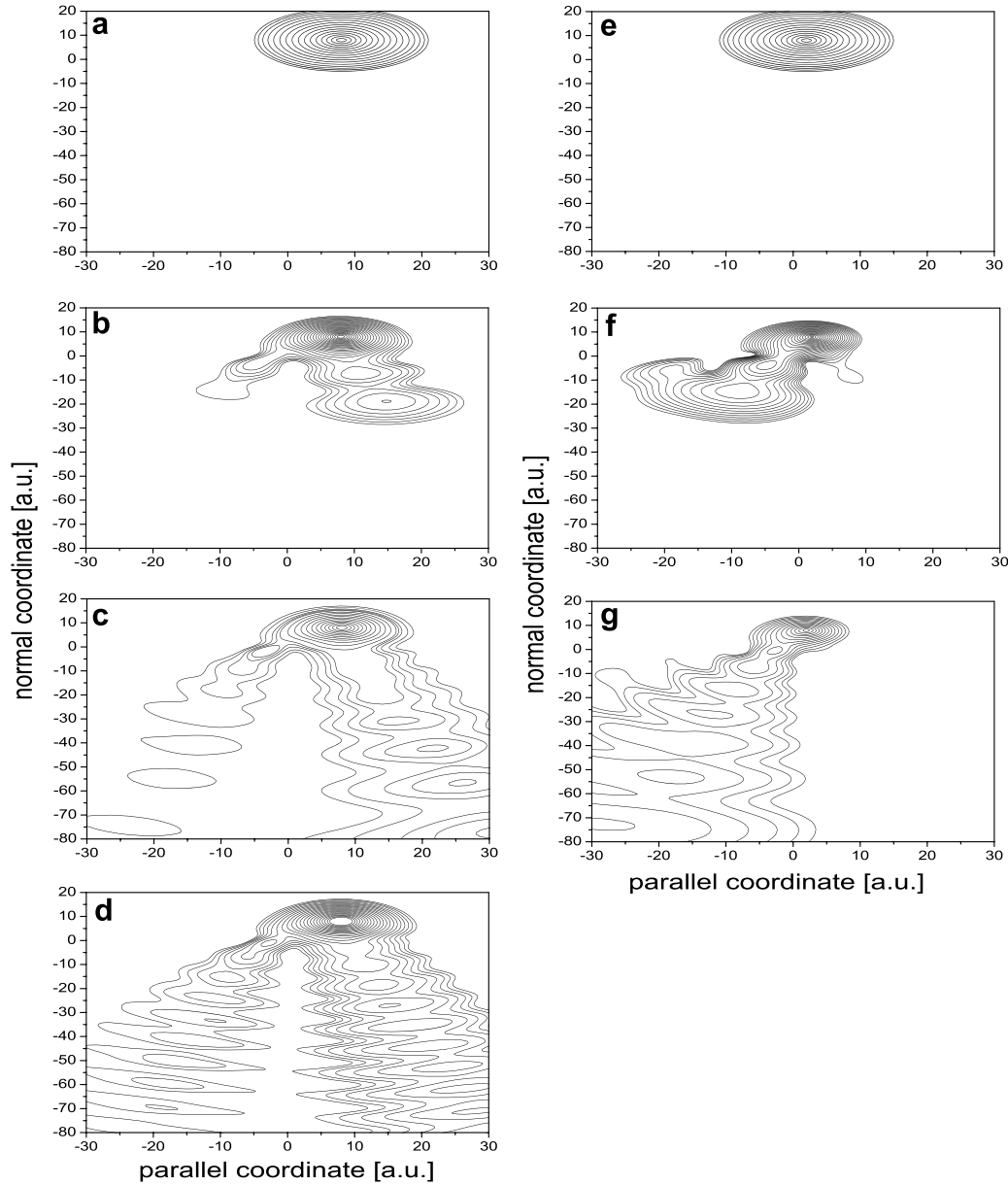


Fig. 8. Contour plot of the logarithm of the modulus of the wave function squared for an electron near a vicinal free electron Cu surface as a function of time. The H^- ion is positioned at $D_{\text{nor}} = 8$ a.u. in front of the optical plane. (a) shows the initial bound state of the ion (at $t = 0$) in the valley between the terraces with parallel coordinate $D_{\text{par}} = 8$ a.u., (b) the electron wave packet after $t = 50$ a.u., (c) at $t = 150$ a.u. and (d) at $t = 600$ a.u. (e) presents the initial state of H^- (at $t = 0$) positioned near a step edge with parallel coordinate $D_{\text{par}} = 2$ a.u., (f) shows the wave packet after $t = 50$ a.u., and (g) after $t = 150$ a.u. The contour spacing is $\approx 0.25, 0.11, 0.17, 0.12$ for figures (a,e), (b,f), (c,g) and (d), respectively.

classical trajectories of the projectile, which reflect specularly on a lower terrace at a fixed distance $D_{\text{step}} < L$ from the step edge. The resonant charge-transfer rates in (6) are related to the instantaneous rate $\Gamma(t)$ as follows. If the shifted affinity level $E_a(t)$ is above the Fermi energy level, the ion is neutralized via electron loss. In contrast, if $E_a(t)$ is below E_F , resonant electron transfer to the metal is forbidden by Pauli's exclusion principle, and charge exchange corresponds to electron capture from the metallic conduction band into the ion level, i.e.

$$\Gamma_{\text{loss}} = \begin{cases} \Gamma, & E_a \geq E_F \\ 0, & E_a < E_F \end{cases}, \quad \Gamma_{\text{cap}} = \begin{cases} 0, & E_a \geq E_F \\ \Gamma, & E_a < E_F. \end{cases} \quad (10)$$

The scattering trajectories are evaluated from the Thomas–Fermi–Moliere string-averaged interatomic potential

$$V_{\text{TFM}}(z') = 2\pi Z_t Z_p n_s a_s \sum_i \frac{a_i}{b_i} \exp(-b_i z' / a_s). \quad (11)$$

z' is the coordinate normal to the terrace, $Z_p = 1$ and $Z_t = 29$ are the atomic numbers of the projectile and target Cu atoms, $a_s = 0.8853(Z_t^{1/2} + Z_p^{1/2})^{-2/3}$ is the Firsov screening length, $n_s = 0.086$ is the number of atoms per unit terrace area, and a_i and b_i are the coefficients given by Moliere [13]. For a given angle of incidence Θ_{inc} of the projectile with respect to the optical surface, we distinguish two types

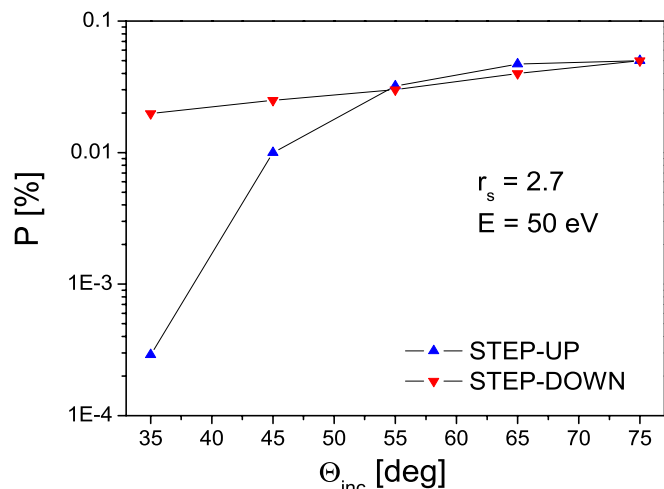


Fig. 9. Survival probability for 50 eV H^- ion after collision with a $(m, n) = (8, 2)$ vicinal Cu surface along “step-up” and “step-down” trajectories as a function of the angle of incidence Θ_{inc} measured with respect to the optical surface plane.

of collision trajectories. Trajectories which approach the step from above are referred as “step-down” and those along which the projectile approaches the step from below

as “step-up”. The total survival probability for a given angle of incidence is obtained after averaging over a finite set of possible turning points on the terrace, i.e., $P = \sum_{D_{\text{step}}} P(\Theta_{\text{inc}}, D_{\text{step}}) / N_{D_{\text{step}}}$, where $P(\Theta_{\text{inc}}, D_{\text{step}})$ is the ion-survival probability for a given angle of incidence, D_{step} is the distance from the upwards step where the reflection occurs and $N_{D_{\text{step}}}$ is the number of trajectories for a fixed Θ_{inc} . We used $N_{D_{\text{step}}} = 7$, corresponding to $D_{\text{step}} = a_0, 2a_0, \dots, 7a_0$ and did not include trajectories that are strongly perturbed by the steps.

Fig. 9 shows the survival probability of 50 eV H^- colliding with a $(m = 8, n = 2)$ vicinal Cu surface as a function of the angle of incidence $\Theta_{\text{inc}} > 20^\circ$. At this kinetic energy the survival probability is small and does not exceed 0.1%. More importantly, ion survival along “step-down” trajectories is always more likely for angles of incidence below $\Theta_{\text{inc}} \approx 50^\circ$.

The substrate-orientation dependence of the H^- survival probability is further analyzed and illustrated in Fig. 10, where the energy of the shifted affinity level along “step-up” (Fig. 10(a)) and “step-down” (Fig. 10(b)) trajectories is shown, together with the corresponding negative-ion-survival probabilities (Fig. 10(c)). The scattering conditions are identical: the trajectories reflect specularly at a mid-ter-

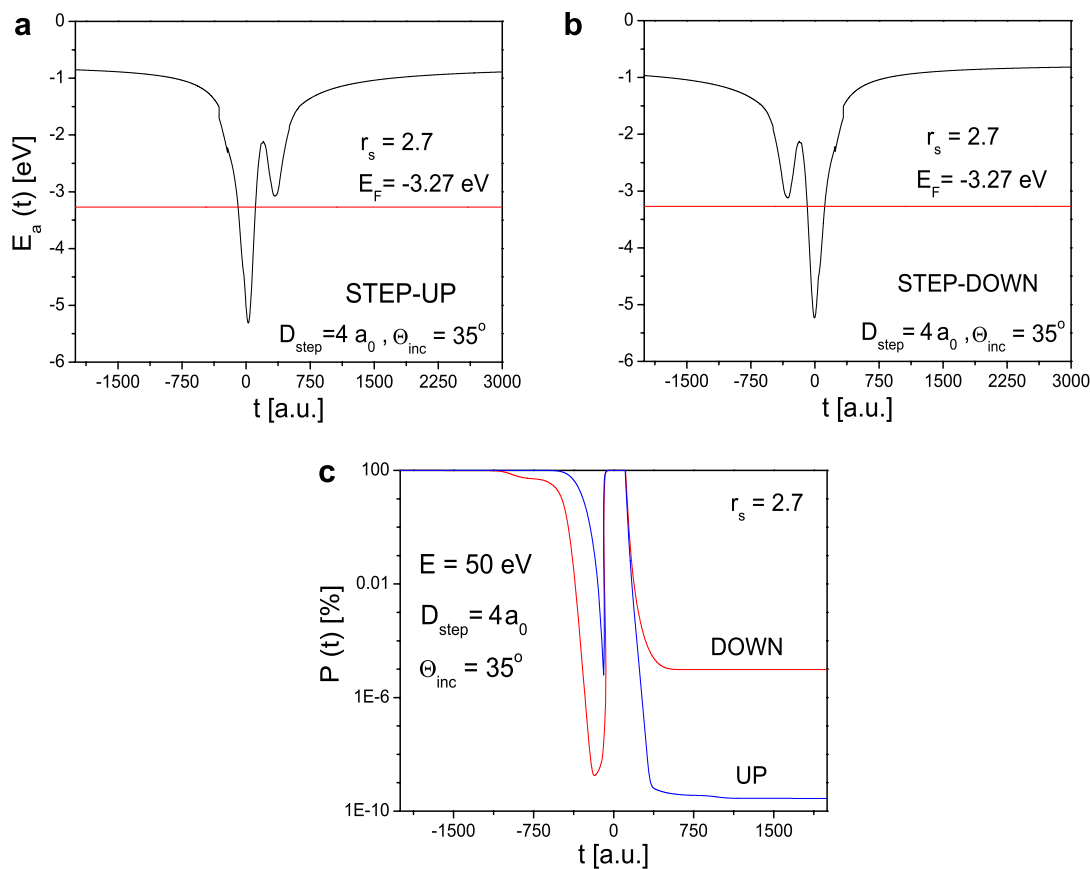


Fig. 10. Energy of the affinity level of H^- during a collision with a $(m = 8, n = 2)$ vicinal Cu surface along “step-up” (a) and “step-down” (b) trajectories. The angle of incidence with respect to the optical plane is $\Theta_{\text{inc}} = 35^\circ$. The reflection occurs near a mid-terrace position $D_{\text{step}} = 4a_0 = 13.64$. The Fermi energy level $E_F = -3.27$ eV is denoted with a solid line. (c) shows the ion-survival probability for negative ions incident with 50 eV as a function of time for the two trajectories.

race position $D_{\text{step}} = 4a_0$. The angle of incidence is $\Theta_{\text{inc}} = 45^\circ$. Fig. 10(c) shows that the survival probability along the “step-up” trajectory is about five orders of magnitude smaller than the “step-down” trajectory. Figs. 10(b) and (c) show the energy level of the affinity resonance and ion-survival probability along the “step-down” trajectory. The ion is completely neutralized before its affinity level crosses E_F , due to the encounter of a step edge prior to reflection from a terrace. After the affinity level has crossed the Fermi energy level, the ion rapidly recovers its initial charge state, due the large capture rate from the conduction band. On the outgoing part of the trajectory, after E_a has crossed E_F from below, the electron loss process is too slow to completely neutralize the ion while it is reflected away from the nearest step edge.

The evolution of the projectile charge state along the “step-up” trajectory in Figs. 10(a) and (c) is quite different. Prior to reflection from a terrace, the projectile charge state is unaffected by the presence of steps. By the time E_a crosses the Fermi energy level, the H^- ion is only partially neutralized. Once E_a is shifted below E_F , the projectile quickly recovers its initial charge state, due to rapid feeding from delocalized conduction band states. On the outgoing part of the scattering trajectory, when E_a shifts across and above E_F , the projectile is completely neutralized due to its close encounter with a step edge, where the electron loss rate is strongly enhanced (cf. Fig. 7(a)). We observe the same trend for other trajectories and surface morphologies and conclude that the “left-right” asymmetry (for incidence angles of $\Theta_{\text{inc}} < 50^\circ$) in the electron transfer at free-electron vicinal metallic surfaces is primarily due to the enhancement of the loss rate on the outgoing part of the “step-up” trajectories.

4. Conclusion

We calculated the static level shift and width of the H^- affinity level in front of a free-electron Cu vicinal surface. From the level shift and width we derived the survival probability of the negative ion for a set of realistic incident trajectories at a kinetic energy of 50 eV. We found that the charge-transfer probabilities exhibit a pronounced “left-right” asymmetry due to enhancement of the electron loss rate along the outgoing part of those scattering trajectories, which approach a step from below. Under otherwise identical conditions, the ion-survival is favored for reflected trajectories which approach a step from above. The origin of this scattering asymmetry is the competition of fast and slow charge transfers between the negative ion and the sur-

face induced by the Smoluchowski effect that redistributes the screening electron density of the substrate near the step edges.

Acknowledgements

This work was supported by the National Science Foundation (Grant PHY03548400) and by the Chemical Sciences, Geosciences, and Biosciences Division, Office of Basic Energy Sciences, Office of Science, US Department of Energy.

References

- [1] J.W. Gadzuk, *J. Phys. Chem. Solids* 30 (1969) 2307.
- [2] J.P. Gauyacq, A.G. Borisov, *J. Phys.: Condens. Matter* 10 (1998) 6585.
- [3] R. Brako, D.M. Newns, *Rep. Prog. Phys.* 52 (1989) 665.
- [4] J. Los, J.C. Geerlings, *Phys. Rep.* 190 (1990) 133.
- [5] M. Maazouz, A.G. Borisov, V.A. Esaulov, J.P. Gauyacq, L. Guillemot, S. Lacombe, D. Teillet-Billy, *Phys. Rev. B* 55 (1997) 13.
- [6] L. Guillemot, V.A. Esaulov, *Phys. Rev. Lett.* 82 (1999) 4552.
- [7] H. Chakraborty, T. Niederhausen, U. Thumm, *Phys. Rev. A* 69 (2004) 052901; H. Chakraborty, T. Niederhausen, U. Thumm, *Phys. Rev. A* 70 (2004) 052903.
- [8] A. Murgaza, A. Mascaraque, V. Pérez, V. Repain, S. Rousset, F.J. García de Abajo, J.E. Ortega, *Phys. Rev. Lett.* 87 (2001) 107601.
- [9] F. Schiller, M. Ruiz-Osés, J. Cordon, J.E. Ortega, *Phys. Rev. Lett.* 95 (2005) 066805.
- [10] J.Y. Park, G.M. Sacha, M. Enachescu, D.F. Ogletree, R.A. RiBeiro, P.C. Canfield, C.J. Jenks, P.A. Thiel, J.J. Sáenz, M. Salmeron, *Phys. Rev. Lett.* 95 (2005) 136802.
- [11] B. Lang, R.W. Joyner, G.A. Somorjai, *Surf. Sci.* 30 (1970) 440.
- [12] B. Obreshkov, U. Thumm, *Phys. Rev. A* 74 (2006) 012901.
- [13] M.T. Robinson, I.M. Torrens, *Phys. Rev. B* 9 (1974) 5008.
- [14] J.S. Cohen, G. Fiorentini, *Phys. Rev. A* 33 (1986) 1590.
- [15] C.A. Utreras-Diaz, *Phys. Rev. B* 36 (1987) 1785.
- [16] A. Chizmeshya, E. Zaremba, *Phys. Rev. B* 37 (1988) 2805.
- [17] R.M. Dreizler, E.K.U. Gross, *Density Functional Theory*, Springer, Berlin, 1990 (Chapter 5).
- [18] P.J. Jennings, R.O. Jones, M. Weinert, *Phys. Rev. B* 37 (1988) 6113.
- [19] N.D. Lang, W. Kohn, *Phys. Rev. B* 1 (1970) 4555.
- [20] R. Smoluchowski, *Phys. Rev.* 60 (1941) 661.
- [21] M. Roth, M. Pickel, J. Wang, M. Weinelt, Th. Fauster, *Appl. Phys. B* 74 (2002) 661.
- [22] X.Y. Wang, X.J. Shen, R.M. Osgood Jr., *Phys. Rev. B* 56 (1997) 7665.
- [23] F. Mehmood, A. Kara, T.S. Rahman, K.P. Bohnen, *cond-mat/0511679*.
- [24] K. Besocke, B. Krahl-Urban, H. Wagner, *Surf. Sci.* 64 (1977) 52.
- [25] M. Weinelt, *J. Phys: Condens. Matter* 14 (2002) R1099.
- [26] A.G. Borisov, A.K. Kazansky, J.P. Gauyacq, *Phys. Rev. B* 59 (1999) 10.
- [27] P. Kürpick, U. Thumm, U. Wille, *Phys. Rev. A* 57 (1999) 1920.